PHYSICAL REVIEW B VOLUME 26, NUMBER 9 1 NOVEMBER 1982

Superconducting properties of Nb/Ge metal semiconductor multilayers

S. T. Ruggiero*
Department of Applied Physics, Stanford University, Stanford, California 94305

T. W. Barbee, Jr.
Department of Materials Science and Engineering, Stanford University, Stanford, California 94305

M. R. Beasley
Department of Applied Physics, Stanford University, Stanford, California 94305
(Received 24 May 1982)

We have made layered superconductors composed of alternating thin films of sputter-deposited Nb and Ge. Individual layer thicknesses range from 5 to 100 Å, each sample containing from 50 to 80 Nb/Ge layer pairs with a fixed thickness ratio, D_{Nb}/D_{Ge}. As revealed by x-ray analysis, the samples have a distinct superlattice structure consisting of amorphous Ge layers and, except for those with $D_{Nb} < 30$ Å, (110) textured polycrystalline Nb layers. Transport studies reveal that each Nb layer itself consists of a clean central portion with damaged regions at the Nb/Ge interfaces. A proximity-effect analysis of the samples indicates that the presence of this damaged Nb interfacial layer largely governs the observed transition temperatures of these multilayers. Measurement of the upper critical fields and fluctuation conductivity have confirmed both the dimensional and the temperature-dependent dimensional crossover effects expected in Josephson-coupled quasi-two-dimensional superconductors. The observed degree of control over interlayer coupling possible with these multilayers suggests they are a model system for the study of quasi-two-dimensional superconductivity.

I. INTRODUCTION

Layered superconductors, materials composed of thin superconducting films separated either by another superconductor or by nonsuperconducting material, have long been of interest because of their unique properties. Both the superconducting and the normal-state properties of such layered systems can differ dramatically from those of bulk materials. It has been clearly demonstrated that the upper critical fields,[1,2] critical currents,[3] and even the transition temperatures T_c (Ref. 4) can be directly influenced by layering. Although interest in layered superconductors is not new, considerable impetus to the field has been provided recently by the successful application of modern thin-film vapor deposition techniques to produce finely layered superconductors of very high physical and structural integrity. In this paper we present a study of a specific multilayer system consisting of alternating sputter-deposited thin films of Nb and Ge. Other workers have studied layered superconductor and normal-metal systems.[5] In the work discussed here, individual layer thicknesses D_{Nb} and D_{Ge} range from 5 to 100 Å at fixed D_{Nb}/D_{Ge} for a given sample. Our goal was to create a model system for studying quasi-two-dimensional (2D) effects in superconductivity. This goal has been met to a very satisfying degree. At the same time a careful study of the structure, transport properties, and transition temperatures of these materials is leading to an improved understanding of the effects of layering on the properties of the individual constituent layers themselves.

Of particular interest in this study is the fact that the dimensionality of a superconducting system has a direct effect upon both the magnitude and temperature dependence of the upper critical field $H_{c2}(T)$. Theoretical models for $H_{c2}(T)$ of layered superconductors[6,7] predict not only large anisotropies but also an actual divergence in the parallel upper critical field in a quasi-2D Josephson-coupled system. The latter can occur in the case where the temperature-dependent perpendicular Ginzburg-Landau coherence length $\xi_z(T)$ approaches the layer repeat distance S of the superconducting films.

Initial attempts to observe such effects focused on the intercalated transition-metal dichalcogenides.

Although large anisotropies,[8] suggestions of temperature-dependent coupling,[9] and other interesting phenomena[10] have been observed in the critical fields of these systems, a satisfactory degree of control over the interlayer Josephson-coupling strength and overall sample integrity has not been achieved. By contrast, systems formed using physical vapor deposition afford fine control over individual film thickness and composition and allow a wide range of materials to be studied. As we have previously reported,[2] it is just this refined control over the interlayer coupling strength that has allowed us to observe clearly the dimensional crossover behavior expected in such systems. Moreover, the interlayer coupling energy is observed to decrease exponentially with increasing Ge layer thickness, consistent with the existence of quantum-mechanical tunneling through the Ge layers.

In this paper we begin our presentation with a discussion of the deposition technique used to produce our multilayers. Following this, results of x-ray and transport characterization studies are presented and then used to develop a model of the physical structure and electrical character of our samples. Next the superconducting properties (T_c and the perpendicular and parallel upper critical fields) are presented and analyzed in terms of the proximity effect for the individual layer properties and of Josephson coupling for the interlayer properties. Finally, the broader implications of this work are addressed and some outstanding unresolved problems are identified.

II. SAMPLE PREPARATION AND CHARACTERIZATION

A. Sample preparation

Our layered composites were prepared by the sequential sputter deposition of Nb and Ge with the use of a technique previously developed by one of us (T.W.B).[11] As depicted schematically in Fig. 1, sapphire substrates were placed on an *in situ* rotating table and alternatively exposed to individual, well-isolated magnetron sources. Not shown in the figure is a shield that provided isolation of the sputtering plasmas from each other. Both the individual sputtering rates (from 1 to 10 Å per sec) and table rotation speed (about 1 rev per min) could be accurately controlled. This system offered the flexibility necessary to produce samples with individual layer thicknesses varying over a wide range. For this study Nb and Ge layer thicknesses (D_{Nb} and D_{Ge}) ranged from 5 to 100 Å and 10 to 100 Å, respectively. For each individual sample on a $\frac{1}{4}\times\frac{1}{4}$ sapphire substrate the ratio D_{Nb}/D_{Ge} was held fixed. Typically 50 to 100 layer pairs were deposited yielding total sample thicknesses of $\simeq 0.5$ μm. In most cases a protective coating of 100 Å of Ge was deposited on the last Nb layer set down. A complementary coating was also deposited on the substrates prior to deposition of the layers.

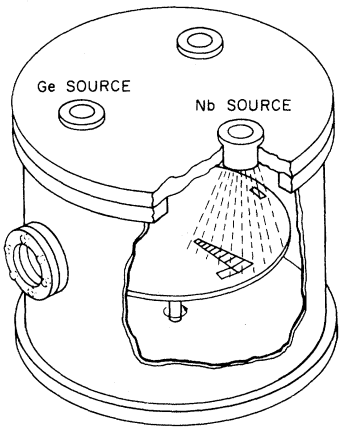

FIG. 1. Schematic of the sputter-deposition apparatus. Sapphire substrates, placed on a rotating table, alternately pass beneath niobium and germanium magnetron sputter sources. Individual layer thicknesses D_{Nb} and D_{Ge}, at a fixed ratio for a given sample, are in the 10–100 Å range.

Preceding each run the sputtering chamber was pumped to 1×10^{-6} Torr, and 3 μm of 99.999% pure argon was bled into the system for sputtering. During sputtering this pressure was maintained by controlling the argon flow rate. The temperature of the rotating substrate turntable was not thermally controlled and, due to the impact of the deposited atoms and radiation from the sources, rose to an estimated 60–80 °C during depositions. Despite its simplicity, this system has regularly and reproducibly provided layered Nb/Ge samples of quite high quality as judged from both their structural and superconducting properties. It has been applied to many other combinations of materials as well.

B. Characterization

1. X-ray analysis

Two x-ray techniques have been employed in the characterization of the Nb/Ge composites: a standard diffractometer and a Read or universal cylindrical camera, which is a modified version of the

Debye-Scherer wide-film camera. The Read camera was used to obtain a semiquantitative overview of the structure of the samples. This instrument is especially valuable in examining films of undetermined structure that are composed of crystallites of unknown orientation and/or lattice parameter. With one exposure a record is made of reflections not only for all angles 2θ between 0 and π but also of reflections through roughly 120° axially in the ϕ direction. As discussed by Read,[12] the utility of this technique is especially evident in the determination of the degree of preferred crystal orientation or film "texture." Representative results are shown in Fig. 2.

The diffractometer provides much more detailed and quantitative information at fixed angle $\phi=0$, i.e., for measuring reflections from lattice planes normal to the film surface. Typical low- and high-angle diffractometer traces are shown in Fig. 3. These measurements served as the primary source of information on the layer thicknesses as we shall discuss in detail later. Moreover, since the composites consist of thin films of alternating materials, the quality of the layering and the layer repeat distance can be established by the low-angle ($2\theta \geq 2°$) superlattice reflections from these planes. An example is shown on the right-hand side of Fig. 3.

One conclusive result from the x-ray studies was the complete lack of evidence for crystalline Ge, indicating that the Ge layers are amorphous, as would be expected for the deposition conditions used. In addition, all samples show a dichotomy in the structure of the individual Nb layers that form in either a highly oriented or randomly oriented state depending on the layer thickness. The former case is illustrated in Figs. 2(a) and 2(b) and the latter in Figs. 2(c) and 2(d). In particular, it is evident from the figure that the sample with $D_{Nb}/D_{Ge}=65$ Å/35 Å, which is typical of our samples with thick Nb layers, exhibits a high degree of preferred orientation with the (110) plane ($2\theta=38.7°$) parallel to the film surface. Each of the lines on the photo has been identified with a bcc Nb lattice reflection as indicated. The width of the lines in the 2θ direction can be attributed, in large part, to broadening due to the finite thickness of the individual Nb layers. The length of the arcs in the ϕ direction characterizes the inherent degree of preferred orientation of the

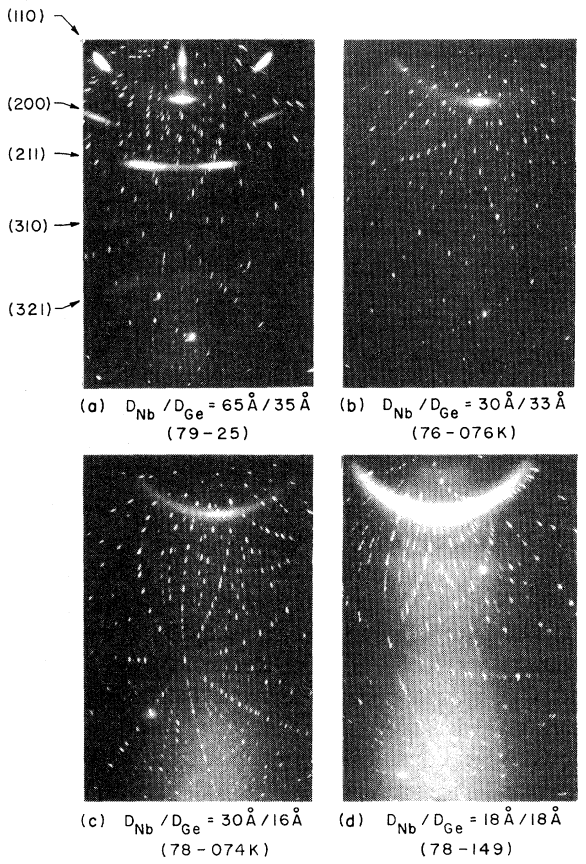

FIG. 2. Representative Read camera x-ray photographs of Nb/Ge composites. The small dots are reflections from the sapphire substrates; the symmetric arcs are identified with bcc Nb lattice reflections. Features of the amorphous Ge layers are not apparent here. The Nb layer are polycrystalline and in samples *A* and *B* exhibit a high degree of preferred orientation of the (110) plane parallel to the film surface. Samples *C* and *D* contain more disordered Nb films.

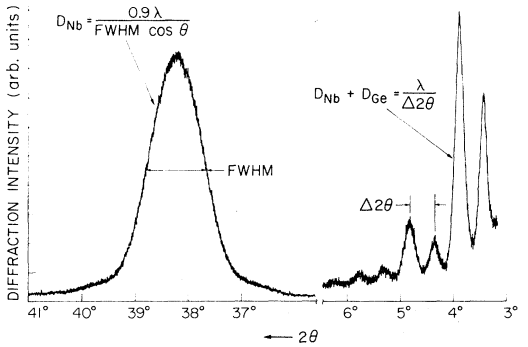

FIG. 3. High- and low-angle diffractometer scans of a typical sample, $D_{Nb}/D_{Ge}=72$ Å/100 Å, containing well-ordered Nb films. Finite-film-thickness effects dominate in the broadening of the Nb (110) peak, the breadth of which is used to calculate the Nb layer thickness, D_{Nb}. The multiple low-angle reflections (observed in all samples) indicate a well-defined superlattice structure and a measure of the layer repeat distance $S=D_{Nb}+D_{Ge}$.

films; in particular, there appears to be a $\pm 5°$ to $10°$ variation in the direction of the (110) reciprocal-lattice vector with respect to the normal to the surface.

Materials with 30-Å Nb layers are shown for comparison. The sample with $D_{Nb}/D_{Ge}=30$ Å/33 Å [Fig. 2(b)] exhibits a degree of preferred orientation comparable to that shown in the sample with $D_{Nb}/D_{Ge}=65$ Å/35 Å but also exhibits a strong diminution of the higher-order reflections. In contrast, the sample with $D_{Nb}/D_{Ge}=30$ Å/16 Å [Fig. 2(c)] displays only a broad arc at $2\theta=37.8°$, with a total absence of all other reflections. By these indications the sample in Fig. 2(c), although clearly composed of Nb crystallites, is disordered. A second sample well within the disordered regime [$D_{Nb}/D_{Ge}=18$ Å/18 Å, Fig. 2(d)] did not show any but the 38.7° Nb(110) reflection, even though overexposed.

The general conclusion arrived at by examining these Read photographs (as well as similar ones on a number of other samples) is that there appears to be no middle ground for the structure of a given sample. Either its constituent Nb films exhibit a high degree of preferred orientation and a number of lattice reflections or are disordered and show a single, broad (110) line. It has been found, without exception, that for $D_{Nb}\gtrsim 30$ Å the films appear ordered and for $D_{Nb}\lesssim 30$ Å they are disordered. As seen above, both types of behavior are present at $D_{Nb}\approx 30$ Å, this thickness apparently serving as a rather well-defined dividing line.

In Fig. 4 we illustrate this pattern exhibited by the composites whose Nb and Ge thicknesses lie in the 5 to 100 Å range. Each sample is represented by a symbol which indicates either high preferential orientation (solid symbols) or disorder (open symbols). This figure is intended not only to emphasize the division in the degree of preferred orientation at $D_{Nb}=30$ Å but also to demonstrate the striking parallel between the pattern seen in the x-ray data and in the residual resistance ratios [$\mathscr{R}$, the room-temperature (300 K) resistance divided by low-temperature (15 K) resistance] of these samples. It is seen in general that for $D_{Nb}\gtrsim 30$ Å there is strong preferential crystal orientation and a $\mathscr{R}>1$, whereas below 30 Å the material is disordered and the $\mathscr{R}<1$. At $D_{Nb}\simeq 30$ Å, either behavior is seen. Even for these samples, however, with one interesting exception, disorder in the x-ray data implied a $\mathscr{R}<1$ and order implied a $\mathscr{R}>1$. The one case at 30 Å that bends this rule is the sample with $D_{Nb}/D_{Ge}=30$ Å/33 Å. As previously discussed

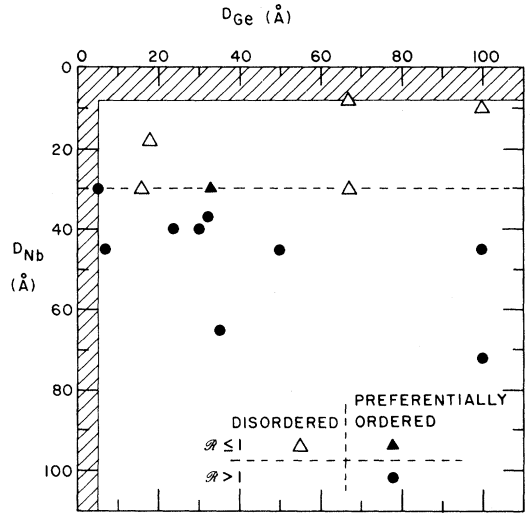

FIG. 4. Map of the Nb layer structure and residual resistance ratio ($\rho_{300\,K}/\rho_{10\,K}$) for all samples studied. There is a distinct break in behavior in the vicinity of $D_{Nb}\simeq 30$ Å. Samples show a high degree of preferred crystalline orientation for $D_{Nb}\gtrsim 30$ Å and a disordered behavior for $D_{Nb}\lesssim 30$ Å. All Nb films with preferred orientation also have a resistance ratio greater than 1.

and displayed in Fig. 2, the Read photograph for this sample, although clearly indicating preferred orientation, did show a strong diminution of higher-order reflections, suggesting a somewhat degraded structural integrity. A full discussion of the resistivities and resistance ratios of these materials is presented later.

Additional information about the structure of these layered composites was supplied by the diffractometer results. Scans of a typical sample with $D_{Nb}>30$ Å ($D_{Nb}/D_{Ge}=72$ Å/100 Å) are shown in Fig. 3. On the right-hand side of the figure, sharp well-defined low-angle peaks are in evidence as is the case for all our samples. Typically from 5 to 10 of these superlattice reflections could easily be seen on the diffractometer, implying a high degree of regularity in the layering.

The angular distance between two adjacent low-angle peaks, $\Delta 2\theta$, is governed by the superlattice spacing $S=D_{Nb}+D_{Ge}$. For sufficiently high order ($n\geq 3$) that refraction effects can be neglected, the applicable small-angle Bragg conditions yield

$$S=(\lambda/2)(\Delta 2\theta)\,, \tag{1}$$

where for the data shown $\lambda=1.54$ Å for Cu $K\alpha$ radiation. Additionally, an upper estimate of the rms deviation δS of the layer separation can be made using a simple variation of the Bragg equation:

$$\delta S/S = \delta 2\theta/2\theta \ , \tag{2}$$

where $\delta 2\theta$ is taken to be the full width at half maximum (FWHM) of a low-angle peak. For these samples, peak widths uncorrected for instrumental broadening indicate $\delta S/S$ values of approximately 5%. This is believed to be a vast overestimate, however.

Shown on the left-hand side of Fig. 3 is a high-angle scan of the Nb(110) reflection. As expected in this case, there is a vastly broadened lattice peak due to the finite film thickness. From the Scherr equation we have

$$D = \frac{K\lambda}{(B-\delta)\cos\theta} \ , \tag{3}$$

where D is the film thickness, B = FWHM, δ is the instrumental broadening ($\simeq 0.15°$), and K is a geometrical constant taken to be 0.9.[13]

The breadth of the high-angle line ($2\theta \simeq 38.7°$) for this and other *ordered* samples could be self-consistently attributed to the finite Nb film thickness. The samples containing disordered Nb layers, on the other hand, while retaining the full integrity of their low-angle superlattice reflections, show a broadening of the (110) line that cannot be consistently accounted for, with equal precision, by finite-film-thickness effects.

2. *Transport properties*

Measurements of the resistance per square ($R_\square$) and residual resistance ratio ($\mathscr{R}$), as defined in Sec. II B 1, were performed on all samples as prepared on $\frac{1}{4}\times\frac{1}{4}$ in.^{2} sapphire substrates using the van der Pauw[14] method. Those samples involved in superconducting critical-field studies were later chemically or plasma etched into geometrically well-defined bridge structures (20 or 300 μm wide) and $R_\square$ was determined by four-point resistance measurements. Electrical connections were made to the as-prepared samples with spring contacts or silver paint, and to the bridges with indium solder. In all cases the precaution was taken to remove any material deposited on the edges of the sapphire substrates. The measured resistivities were found to be independent of geometry and technique. All resulting values of $R_\square$ given in the text and listed in Table I are defined as the resistance per square of individual Nb layers: that is, the value obtained by multiplying the $R_\square$ of the composite by the number of Nb layers. Although the temperature dependence of the resistivity was not studied in quantitative detail, in general it was observed to be monotonic (i.e., continually increasing or decreasing depending on the $\mathscr{R}$). For the metalliclike samples ($\mathscr{R} < 1$), there was a broad range of temperatures at low temperatures over which the resistivity was temperature independent. For those samples with $\mathscr{R} > 1$, the dominant part of the resistivity increase occurred at low temperatures.

To illustrate the dependence of the resistivity on layer thickness, the conductance per square $G_\square$ ($\equiv 1/R_\square$) for our composites (irrespective of Ge thickness) is plotted against Nb film thickness in Fig. 5. The behavior of the data is revealing. We

TABLE I. Material parameters of the Nb/Ge composites.

Samples	D_{Nb}/D_{Ge} (Å/Å)	Number of Nb layers	T_c (K)	$R_\square$ (Ω layer)	$\mathscr{R}$
78-075K	30/5	84	4.87	176	1.16
78-075S1	45/7	84	5.9	65.3	1.41
78-146S2	40/24	130	4.15	100	1.18
78-135S1	40/30	60	3.61	135	1.15
78-076L	30/33	50	3.57	413	0.945
79-25S3	65/35	50	6.88	25.0	1.91
79-26S2	37/32	50	4.94	91.6	1.37
78-076	45/50	50	4.98	69.6	1.36
76-168	100/100	100	5.27	50	1.3
78-074L	30/16	72	3.88	453	0.975
78-071S2	45/100	50	4.1	93.1	1.27
78-070S1	72/100	50	6.1	28.0	1.57
78-071L	30/67	50	2.5	411	0.926
78-072A	36/100	80	3.1	244	~1
78-149B	18/18	200	3.2	637	0.951
79-149L	12/12	200	3.1	692	0.888
78-073	10/100				0.953

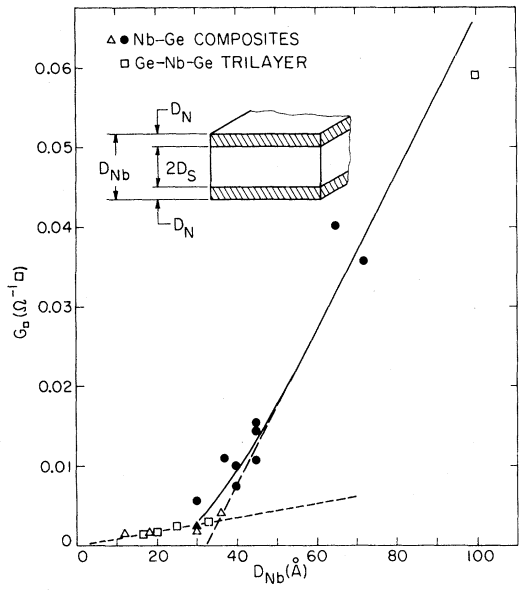

FIG. 5. Low-temperature conductivity per square vs niobium layer thickness. Symbols are defined in Fig. 4. The data for thicker layers are distinctly offset from the origin. By assuming Nb layers are composed of a central region of well-ordered material of 9.8 $\mu\Omega$ cm on either side of which is a total of 26 Å of disordered material of 114 $\mu\Omega$ cm (see inset), the data can be well accounted for.

see that $G_\square$ vs D_{Nb} approaches a linear behavior at large D_{Nb}, as expected for a film of uniform resistivity but with a displaced origin. For $D_{Nb} \lesssim 30$ Å linear behavior is also seen but the slope implies a much lower conductivity. Although a depression in conductivity is expected due to boundary scattering in just this region, a simple calculation shows that it does not account for the observed behavior. In fact, to first order the data suggest a simple offset in Nb layer thickness of ~ 30 Å, independent of the Ge layer thickness. Consequently, we envision the metal layers as being composed of homogeneous, electrically continuous Nb on either side of which (or on one side of which) is a thin layer of degraded, low-conductance material. From the slopes of lines in Fig. 5 we infer resistivities $\rho = 9.8$ and 114 $\mu\Omega$ cm for the two types of material. In view of the x-ray data discussed earlier, the structure of these materials implied by the transport measurements is quite reasonable. We recall that the Read camera results of Fig. 2 show a striking degradation in the texture of the layers for $D_{Nb} \leq 30$ Å.

There are several possibilities that might explain the existence of a damaged layer of fixed thickness as proposed above. One candidate is an interfacial "mixing" of Nb and Ge atoms due to a finite fraction of sputtered atoms with a high kinetic energy. A second possibility is suggested by recent results of multilayer depositions in the presence of oxygen in the sputtering system used to produce our Nb/Ge composites. It appears that as samples pass into or from beneath a given source, they encounter a region of relatively low deposition rate. Because the deposition rate is lower in these regions, the top and bottom of a given layer are more susceptible to contamination by gas impurities from the chamber. This explanation is particularly viable considering the exceptional gettering capability of Nb. Finally, the damaged region may result from imprecise film growth as each new Nb layer is nucleated. In this case the degraded region would all be on one side. Of course, combinations of the above-mentioned effects are also possible.

One second-order characteristic of the data in Table I and Fig. 5 is a small systematic dependence of $G_\square$ on D_{Ge}. For film thicknesses $D_{Nb} > 30$ Å careful examination of the data reveal a small decrease in $G_\square$ at fixed D_{Nb} as D_{Ge} increases. This effect is consistently larger for thinner Nb layers until one moves into the $D_{Nb} \leq 30$ Å regime; here the films have a much smaller overall $G_\square$, which appears independent of D_{Ge}. This subsidiary effect does not, however, substantively alter our basic picture that these materials are comprised of well-defined layers of Nb, which themselves are formed from a relatively clean layer of Nb adjacent to disordered interfacial Nb, separated by layers of *a*-Ge that are essentially insulating.

III. SUPERCONDUCTING PROPERTIES

A. Critical temperatures

In general it is found that the transition temperatures T_c of our composites depend upon both the Nb and Ge layer thicknesses. These dependencies are illustrated in Fig. 6 where representative data are shown for T_c as a function of D_{Ge} at various fixed values of D_{Nb}. Note that T_c decreases both as D_{Nb} decreases and, for fixed D_{Nb}, as D_{Ge} increases. One would like to self-consistently understand both of these effects.

Clearly there are significant changes in T_c as we vary the respective layer thicknesses. One possible origin of these effects is the essentially passive influence on the superconducting order parameter associated with the proximity effect. Clearly, given the nonuniform nature of the Nb layers described in

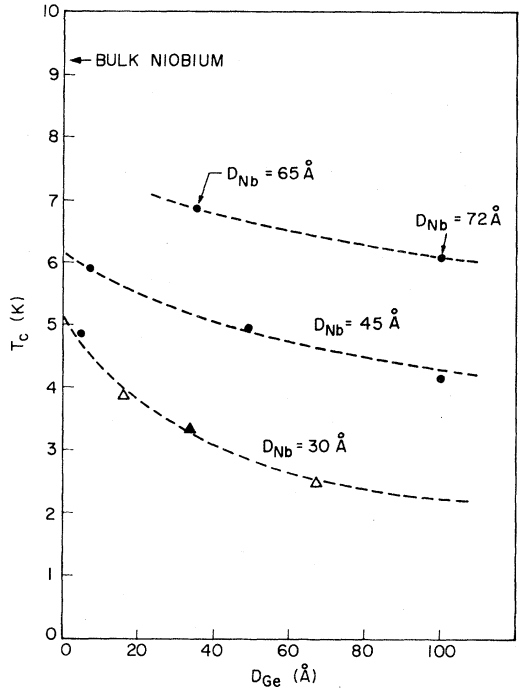

FIG. 6. Critical temperature vs D_{Ge} for three series of samples of different D_{Nb}. Increasing D_{Ge} at fixed D_{Nb} affects a substantial depression of T_c.

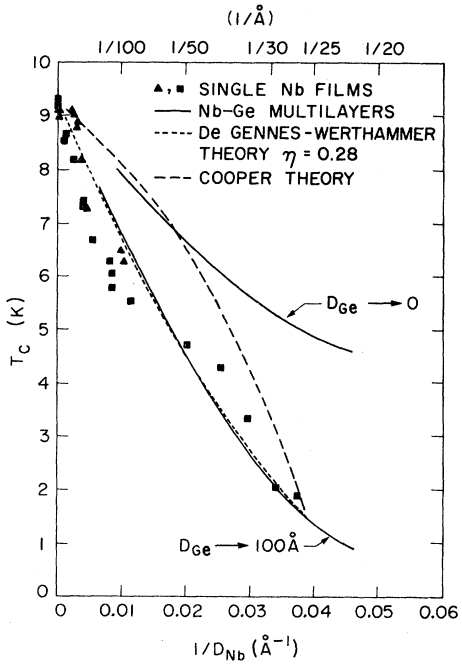

FIG. 7. Solid lines depict T_c vs $1/D_{Nb}$ for layered composites in the limits of large (100 Å) and zero Ge thickness between Nb layers as extrapolated from the data of the previous plot and for other less complete series at different D_{Nb}. The solid points are the results for single, sputter-deposited Nb films reported by Wolf *et al.* (■) and Mayadas *et al.* (▲), Ref. 15. Note the good correspondence between the single-film and $D_{Ge}\rightarrow 100$ Å Nb/Ge results. Dotted lines are proximity-effect calculations for a two-component model of the Nb films which assumes the existence of a fixed thickness of low-T_c, low-conductance interfacial material.

Sec. II, there must be some influence on T_c due to a proximity effect within the individual Nb layers. At the same time there can be changes of the normal-state material properties of the Nb layers relevant for superconductivity associated with the layering. Finally, new effects arising from coupling between the layers are conceivable. As we shall see it is not currently possible to understand all aspects of the behavior illustrated in Fig. 6. However, considerable progress can be made as discussed below.

In order to characterize more simply the dependence of T_c on D_{Nb} and D_{Ge}, we have examined the limiting values of T_c observed as $D_{Ge}\rightarrow 0$ and $D_{Ge}\rightarrow 100$ Å. The results are shown in Fig. 7 (solid curves) for the data of Fig. 6 along with those from other less complete series at different D_{Nb}. The trends indicated are representative of the behavior exhibited by all of our samples. The solid points are data taken from previous studies of single thin films of sputter-deposited niobium.[15] The correspondence between the single-film data and those for the layered materials as $D_{Ge}\rightarrow 100$ Å confirms that the Ge layers are in fact electrically passive and that the apparent increase of T_c as $D_{Ge}\rightarrow 0$ may be genuine and not a trivial result of a proximity effect with the Ge layer. This conclusion is also consistent with the known, low conductivity of *a*-Ge at low temperatures, which according to the conventional proximity-effect models is far too low for the Ge to influence significantly the T_c of the Nb layers through this mechanism.

Consider now the data in the thick-Ge limit. Given that the Ge is electrically passive (i.e., like a vacuum) and the fact that the pristine part of each Nb layer has a low, constant resistivity $\rho\simeq 10$ $\mu\Omega$ cm, it is evident that the reduction of T_c seen in this case as D_{Nb} decreases almost certainly arises (at least in part) due to a proximity effect with the degraded Nb layer. It is not known, however, what fraction of the 30 Å of disordered Nb resides at the top (bottom) of the Nb layers. For simplicity we shall assume that it is equally distributed, although this is not an essential assumption and does not significantly alter our results. Under this assumption,

by symmetry, the proximity-effect analysis for our multilayered composites is equivalent to analyzing a single, fictitious bilayer composed of half of each individual layer, i.e., half the central portion of the film and one damaged region with vacuum interfaces on each side.

The theory of the proximity effect for such a bilayer is summarized in Appendix A. Taking $2D_N = 26$ Å and $2D_S = D_{Nb} - 26$ Å, to calculate T_{cNS} (D_{Nb}) requires knowledge of T_{cS}, T_{cN}, $\xi_S(0)$, $\xi_N(0)$, and the parameter η that parametrizes the boundary conditions on the superconducting order parameter at the S/N interface. Note that here we take the subscript N to denote the damaged Nb layer with the lower T_c. Observing that $T_{cS} = 9.25$ K and $T_{cN} \simeq 1.5$ K from Fig. 7, and taking $\xi_S(0) \simeq 85$ Å and $\xi_N(0) \simeq 110$ Å from the perpendicular critical-field measurements discussed below, we have calculated T_{cNS} from the de Gennes–Werthammer theory as a function of D_{Nb} for various values of η. The best fit is shown by the lower dashed line in Fig. 7. As seen in the figure the fit is quite satisfactory and yields $\eta = 0.28$. According to de Gennes, $\eta = \sigma_N/\sigma_S \simeq 0.1$ for our samples, in reasonable agreement with the fitted value, considering the lack of complete theoretical certainty as to the most appropriate representation of this parameter.[16] Also shown is a fit to the Cooper limit formula, which assumes the pair potential to be constant in the S and N regions and where we have taken[17]

$$\frac{N_N^b(0)}{N_S^b(0)} \simeq \frac{\lambda_N}{\lambda_S} = 0.5 .$$

We return in Sec. IV to the question of the increase in T_c in the limit of small D_{Ge}.

B. Critical fields

1. *Perpendicular critical fields*

Figure 8 shows typical results for the perpendicular upper critical fields for a series of Nb/Ge composites. From left to right the samples correspond to Nb thickness from 30 to 45 Å. Since the field is perpendicular to the films and we are in the dirty limit ($\xi_0/l > 1$), we have used the standard Werthammer, Helfand, and Hohenberg (WHH) theory[18] to generate fits to the data as shown. One difficulty in this procedure arises because of the so-called "positive curvature" exhibited to some degree by all of our samples. That is, there is an obvious deviation from linearity near T_c which has a positive

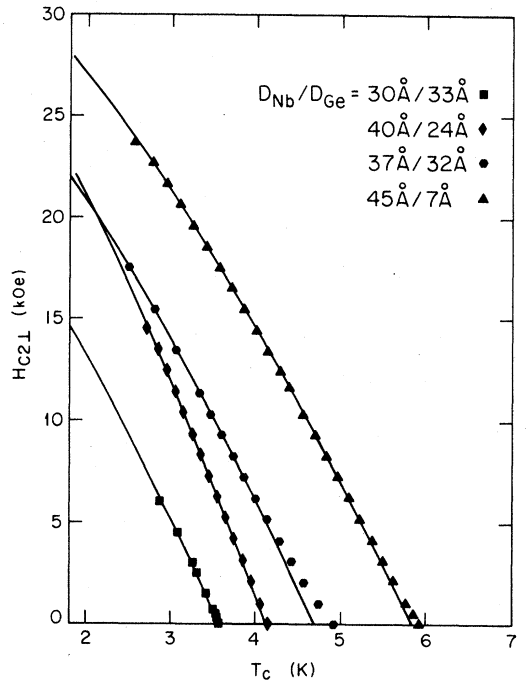

FIG. 8. Perpendicular upper critical fields of a series of Nb/Ge composites of increasing T_c and Nb-layer thickness.

second derivative.

Some degree of positive curvature appears to be a phenomenon common to all layered superconductors, both natural and synthetic. The universality of this behavior in the layer dichalcogenides was first pointed out by Woollam *et al.*[10] One aspect of this phenomenon in our materials, which is important to the present discussion, is that, unlike the layered compounds, the phase boundaries of the parallel upper critical fields of our synthetically layered materials (see below) do not exhibit positive curvature and extrapolate to $T_c(H=0)$ as determined from the resistive transition. This also appears to be the case in the related Al/Ge composites of Haywood and Ast[1] in which positive curvature in the perpendicular direction was also clearly evident. These results suggest that $T_c(H=0)$ truly represents the BCS critical temperature of these samples and that positive curvature is not associated in any trivial way with broadening of the transition due to sample inhomogeneity. Indeed, as we have noted previously,[2] the amount of positive curvature is found to increase as the layers are decoupled, implying that it may be a property of isolated, individual layers.

Unfortunately, positive curvature somewhat com-

plicates the determination of $(dH_{c2}/dT)_{T_c}$, from which the Ginzburg-Landau (GL) coherence length is calculated. Since the critical-field curves cannot be fitted by starting at the observed T_c's, a somewhat reduced value is used, along with an effectively higher critical-field slope. It is felt that this enhanced slope, which is employed in fits to the WHH theory, overestimates the true slope, especially in the cases where the curvature is large. Therefore, an average slope was employed that included additional points at lower fields and more closely resembled a straight-line fit near the measured T_c. These average slopes were typically smaller by $\simeq 10\%$ than the WHH fitting result. The critical-field slopes determined in this fashion are listed in Table II for all the samples studied, along with similar data for the parallel direction to be discussed below. In Fig. 9 we show $(dH_{c2\perp}/dT)_{T_c}T_{cNS}$ as a function of $D_{\rm Nb}^{-1}$.

As seen in this figure, $(dH_{c2}/dT)T_{cNS}$ slightly decreases with increasing $D_{\rm Nb}^{-1}$. The two limits ($D_{\rm Nb}\rightarrow\infty$ and $D_{\rm Nb}\rightarrow 26$ Å) should reflect the behavior of the clean and damaged region of our Nb layers, respectively. Using the standard relation

$$\xi^2(0)=\Phi_0\left[2\pi\frac{dH_{c2}}{dT}T_c\right]^{-1}, \tag{4}$$

we obtain the values $\xi_S(0)=85$ Å and $\xi_N(0)=110$ Å used in the fits of T_c discussed above. As discussed in the Appendix by assuming η is not field dependent, the dependence of $(dH_{c2}/dT)T_{cNS}$ on $D_{\rm Nb}$ expected from the proximity effect can be readily calculated [Eq. (A7)]. The results of this calculation are shown in the figure, taking $\eta=0.28$ as determined from the T_{cNS} data in Fig. 7. The agreement between the proximity-effect theory and the data is satisfactory.

In Table II we list the value of $\xi(0)$ determined from Eq. (4) for all samples. Because of the layered nature of the Nb layers themselves, the values given represent an effective coherence length. They can be interpreted as the in-plane value that would appear in a GL equation for the layer in which the GL order parameter represented an average value over the full width of the layer. Such an average point of view is legitimate since for the samples listed $2D_N<\xi_N(0)$ and $2D_S<\xi_S(0)$, and therefore the order parameter has only a moderate spatial variation across the S or N regions.

2. *Parallel critical fields—effect of Josephson coupling*

One of the primary reasons for the interest in synthetically layered superconducting composites lies in their potential for exhibiting the novel features expected in Josephson-coupled, quasi-two-dimensional superconductivity. The theory of the parallel critical field in such systems is highly developed.[7] Previous experiments on the naturally occurring layered compounds aimed at studying these effects have been generally hampered by material problems and only qualitative or perhaps semiquantitative tests of the theory have been possible.[9] By contrast, as we have reported previously, our Nb/Ge multilayer composites appear to be a model system for such studies.[2]

The theory of the parallel critical field has been discussed extensively in the past, and we only review its main features here. For a system of Josephson-coupled superconducting layers the kinetic energy of the system is given within the Ginzburg-Landau approximations as

$$\epsilon_{\rm GL}=\frac{\hbar^2}{2m}(k_x^2+k_y^2)+\eta_J(1-\cos k_z S), \tag{5}$$

TABLE II. Upper critical-field parameters of the Nb/Ge composites.

Sample	$D_{\rm Nb}/D_{\rm Ge}$ (Å/Å)	T_c (K)	$(dH_{c2\perp}/dT)_{T_c}$ (kOe/K)	$(dH_{c2\parallel}/dT)_{T_c}$ (kOe/K)	$(M/m)^{1/2}$	$\xi(0)$ (Å)	$\xi_z(0)$ (Å)	$\frac{4}{\pi}\left[\frac{\xi_z(0)}{S/2}\right]$
78-075K	30/5	4.87	11.2	24.8	2.21	77.7	35.1	5.15
78-075S1	45/7	5.9	7.58	22.2	2.93	85.8	29.3	1.62
78-146S2	40/24	4.15	10.2	34.4	3.37	88.2	26.1	0.85
78-135S1	40/30	3.61	9.18	39.3	4.28	99.7	23.3	0.56
78-076L	30/33	3.57	9.4	29.0	3.08	99.0	32.1	1.32
79-25S3	65/35	6.88	6.5	57.9	8.91	85.8	9.63	0.047
79-26S2	37/32	4.94	7.9	89.0	11.3	91.8	8.15	0.071
78-076	45/50	4.98	6.75	∞	∞	99.0	0	0

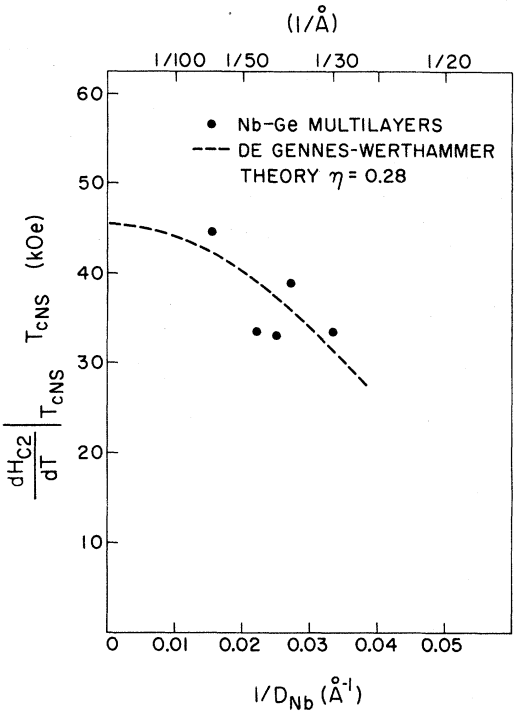

FIG. 9. Measured values of $(dH_{c2\perp}/dT)_{T_{cNS}}T_{cNS}$ vs $1/D_{\mathrm{Nb}}$ for composites with $D_{\mathrm{Ge}} \gtrsim 30$ Å. The theoretical result based on the proximity-effect theory, Eq. (A7), from which the values $\xi_S(0)=85$ Å and $\xi_N(0)=110$ Å are determined, is shown as the dotted line.

where η_J is the coupling energy and S is the layer repeat distance. In the case where the superconducting order parameter varies slowly on the scale of S, Lawrence and Doniach[6] have developed an effective-mass model where

$$M=\frac{\hbar^2}{\eta_J S^2}\ , \tag{6}$$

for motion perpendicular to the layers. Therefore the mass of the superconducting electrons is effectively increased, giving rise to anisotropic behavior. This model is equivalent to defining a "perpendicular" coherence length $\xi_z(T)=(m/M)^{1/2}\xi(T)$, where ξ is the usual (in our case the effective) GL coherence length for electron motion confined to a single layer. Consequently, for magnetic fields applied parallel to the layers,

$$H_{c2||}(T)=\Phi_0/2\pi\xi(T)\xi_z(T)\propto(1-T/T_c)$$

near T_c.

If, on the other hand, the layers are sufficiently decoupled, the effective-mass model breaks down at low temperatures and interesting results are expected. More specifically, as the temperature is reduced, $\xi_z(T)$ decreases and can actually approach the layer repeat distance S at which point the system makes a transition into the so-called quasi-2D or Josephson regime. Here the electron coupling manifests itself in a manner akin to that in a Josephson tunnel junction. A detailed account of the behavior expected in this regime reveals that

$$H_{c2}(T)\propto 1/[1-2S^2/\xi_z^2(T)]^{1/2}\ .$$

This striking result predicts a divergence in the parallel upper critical fields of these systems at a temperature T^* given by the relation

$$\xi_z(T^*)=S/\sqrt{2}\ . \tag{7}$$

For a real system this divergence is eliminated by pair breaking within the individual layers (e.g., due to Pauli paramagnetic limiting or the effect of finite-film thickness). In general T^* represents a dimensional crossover temperature for $H_{c2||}$.

In order to test these theoretical predictions, careful parallel critical-field data were taken on the samples listed in Table II. Samples with much greater D_{Ge} invariably showed critical fields with $H_{c2||}\propto(T_c-T)^{1/2}$ appropriate to isolated thin films. Note that as can be shown in the Cooper limit this temperature dependence is expected, even though the individual Nb layers are not homogeneous.[19] The measured critical-field slopes at T_c are listed in the table and data on three typical samples with roughly fixed D_{Nb} but varying D_{Ge} shown in Fig. 10. The perpendicular critical fields are also shown for comparison.

The first thing to note here is the high degree of anisotropy between the parallel and perpendicular directions; also, the anisotropy clearly increases with increasing Ge thickness as expected. In detail, we see that for $D_{\mathrm{Ge}}=7$ Å, $H_{c2||}(T)\propto T_c-T$ near T_c, which is a signature for coupled or 3D behavior. Furthermore, increasing D_{Ge} to 50 Å gives $H_{c2||}\propto(T_c-T)^{1/2}$ near T_c, which implies fully decoupled 2D behavior. More interestingly, for the sample with $D_{\mathrm{Ge}}=35$ Å we do indeed see the dimensional crossover behavior expected from theory. That is, near T_c, $H_{2c||}(T)\propto T_c-T$, whereas further from T_c the expected upturn in $H_{c2||}(T)$ is clearly observed. Moreover, it occurs precisely at the predicted dimensional crossover temperature T^* for this particular sample ($T^*/T_c=0.98$). Finally, at lower temperatures $H_{c2||}(T)$ approaches the phase boundary for fully decoupled (2D) layers. The solid curves shown are calculated from the full Klemm, Luther, and Beasley theory[7] including an intralayer pair breaker proportional to H^2. A second sam-

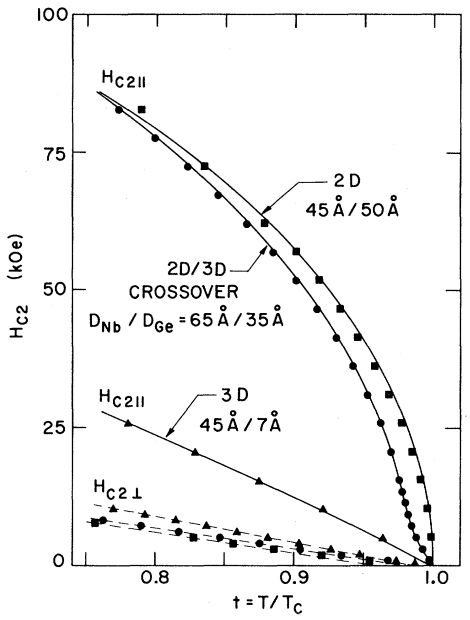

FIG. 10. Upper critical fields near T_c including a sample exhibiting an upturn in $H_{c2\|}(T)$. Systematically increasing the Ge-layer thickness between 2D Nb layers affects a progression from anisotropic 3D behavior $[H_{c2\|}(T)\sim(1-t)]$ to "crossover" behavior and finally to decoupled, 2D behavior $[H_{c2\|}(T)\sim(1-t)^{1/2}]$. Solid lines are from the Josephson-coupling theory.

ple ($D_{Nb}/D_{Ge}=37$ Å /32 Å) showed the same behavior, again in exact accord with theory. As reported earlier[2] these samples also showed the expected dimensional crossover behavior in their fluctuation conductivity above T_c, again with a dimensional crossover temperature in agreement with theory.

3. Fitting parameters

The quantities that enter into the Josephson-coupling theory for $H_{c2\|}(T)$ are $\xi_z(0)$, S (from which the coupling parameter $r\equiv(4/\pi)[2\xi_z(0)/S]^2$ can be calculated), T_c, and the parameters necessary to determine the strength of the intralayer (2D) pair breaking. The intralayer pair breaking is believed to arise from a combination of Pauli limiting and thin-film orbital effects. In the dirty limit appropriate for our samples, both of these mechanisms lead to a pair-breaking parameter proportional to H^2. Hence one cannot, in general, separate their effects. The situation is further complicated by the *NSN* "trilayer" structure nature of the individual Nb layer in our multilayers. The orbital effects under such conditions have been analyzed in the Cooper limit (and the functional dependence of the pair breaker remains the same) but no general theory has been worked out. We believe that as long as $D_N \ll \xi_N(0)$ and $D_S \ll \xi_S(0)$, in general the pair breaker will be proportional to H^2, and in our fits to $H_{c2\|}$ we have simply treated the coefficient of the H^2 term as an adjustable parameter. The values obtained are in reasonable agreement with estimates based on the measured material parameters of the Nb layers and assuming the layers are homogeneous. Also, note that this uncertainty in the intralayer pair-breaking parameters has very little influence on the quality of the fit in the dimensional crossover regime as shown in Fig. 10.

4. Anisotropy in the effective masses and interlayer coupling strengths

From the critical-field slopes listed in Table II it is possible to calculate the effective-mass ratio M/m and the results are included in that table. In Fig. 11(a) this mass ratio is shown as a function of

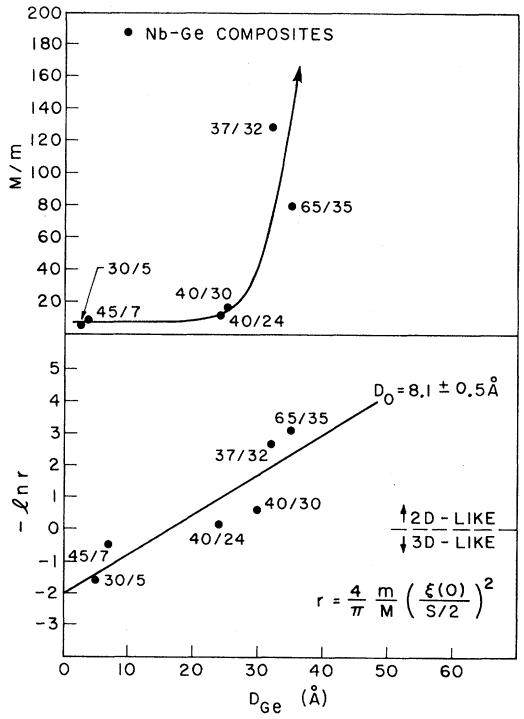

FIG. 11. Effective-mass ratio M/m and logarithm of the coupling parameter r as a function of D_{Ge}. The Nb layers rapidly decouple in the vicinity of $D_{Ge}\sim 30$ Å. The linear dependence of $\ln r$ with D_{Ge} implies an 8-Å characteristic tunneling length in the amorphous Ge layers.

D_{Ge}. The sharp rise at $D_{Ge} \simeq 30$ Å is clearly evident.

More important is the behavior of the interlayer coupling strength

$$\eta_J = \hbar^2/MS^2 = (\pi r/8)[\hbar^2/2m\xi^2(0)] .$$

This relation reflects the fact that the theoretical parameter r has the interpretation as the ratio of interlayer coupling energy to the energy scale for spatial variations of the order parameter within a given layer. Since $\xi(0)$ is roughly constant for our samples, we can determine the dependence of η_J on D_{Ge} from the measured quantity r. This is shown in Fig. 11(b) where we see that $r \propto \exp(-D_{Ge}/D_0)$, where the characteristic length $D_0 \simeq 8$ Å is consistent with the idea of electron tunneling through the Ge layers. A similar length (~ 10 Å) has been found by Rudman and Beasley for tunneling through amorphous Si.[20]

More difficult to interpret have been the data of Fig. 12. Here we show the results for the angular dependence of $H_{c2}(T)$ near T_c for samples which showed both fully coupled, 3D behavior (D_{Nb}/D_{Ge}=45 Å/7 Å) and decoupled 2D behavior (D_{Nb}/D_{Ge}=45 Å/50 Å) as previously discussed. Although the latter conforms nicely to the Tinkham result[21,22] appropriate to 2D thin films, the data for the 3D sample is not in complete accord with the usual effective-mass model for a well-coupled layered system.[6] This theory predicts a zero slope for $[dH_{c2}(\theta)/d\theta]_{\theta=90°}$, while the data form a distinct cusp at $\theta = 90°$, i.e., where the field is parallel to the layer. Similar behavior in the angular dependence of the Nb/Cu system[23] has led to the interpretation that, in a system of well-coupled layers, H_{c3} (surface state) effects may come into play and lead to a sharpening of $H_c(\theta)$ near $\theta = 90°$. As is well known[24,25] the angular dependence of $H_{c3}(\theta)$, like thin films, has a sharp cusp at $\theta = 90°$. Since for our systems, $H_{c2||}(T)/H_{c2\perp}(T) > 1.7$, a surface state would presumably occur in conjunction with other anisotropic effects. In addition, the effects of finite film thickness, although accounted for explicitly in describing the $H_{c2||}(T)$ phase boundary, are not included in the simple effective-mass model—an omission which may be relevant in regard to the angular dependence of the composites. Notwithstanding the unresolved nature of this perhaps substantive issue, the assumption has been made that the observed behavior of $H_{c2||}(T)$ near T_c is representative of the appropriate perpendicular Ginzburg-Landau coherence length as discussed within this paper.

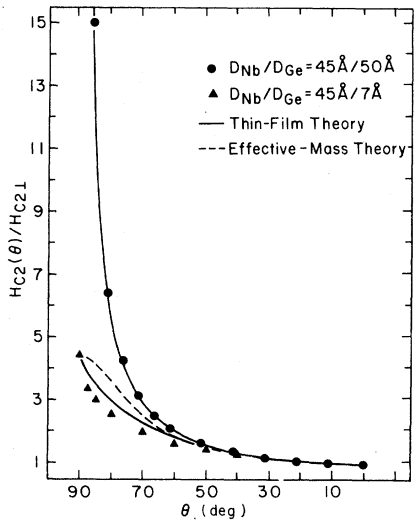

FIG. 12. Representative angular dependence of $H_{c2}(T)$ near T_c for the Nb/Ge composites. A sample with fully decoupled Nb layers D_{Nb}/D_{Ge}=45 Å/50 Å shows good agreement with the Tinkham result (Ref. 21) for single thin films. However, a sample which exhibited coupled, 3D behavior of $H_{c2||}(T)$, D_{Nb}/D_{Ge} =45 Å/7Å, has a dependence of $H_{c2}(\theta)$, which is not in full agreement with the expected effective-mass result. Moreover, the rate of change of $H_{c2}(\theta)$ near parallel orientation is sharper even than that predicted by the thin-film theory.

IV. CONCLUSIONS AND SUMMARY

In conclusion, state of the art sputtering techniques have been employed to produce layered Nb/Ge composites which represent a "model system" for studying dimensional effects in superconductivity. The suitability of these materials for such a role rests, ultimately, on the ability to accurately and reproducibly tailor layer thickness and periodicity in appropriate regimes, and the overall integrity of these systems in those regimes. In our composites, niobium layers can be produced with both thicknesses less than $\xi(0)$, the Ginzburg-Landau coherence length, making them intrinsically two dimensional (2D), and with critical temperatures T_c in a conveniently accessible range (>4 K). By increasing the germanium thickness D_{Ge} between the 2D niobium layers, the degree of interlayer coupling can be systematically decreased. Individual samples have been produced in which 3D, quasi-2D, and purely 2D behavior has been attained and confirmed by measurements of both the parallel

upper critical fields and fluctuation conductivity.[2] Separately, in other layered systems, both 3D and 2D behavior has been observed. It is, however, the attainment of the intermediate, quasi-2D, state of layer coupling which is most representative of the unique superconducting properties of the layered Nb/Ge composites.

In the quasi-2D state the superconducting dimensionality of the system is now temperature dependent. This is most vividly and dramatically manifested in the behavior of the parallel upper critical fields which show a linear 3D behavior near T_c crossing over, at a lower temperature T^* defined as $\xi_z(T^*)=S/\sqrt{2}$, to a 2D (decoupled) state in exact agreement with the theory for Josephson-coupled layers. In a broader view, this behavior represents a transformation from the usual Abrikisov vortex lattice near T_c to a unique and hitherto unexplored Josephson-vortex lattice in the vicinity of T^* which lacks the usual dissipative vortex cores (which now lie, in a sense, between Nb layers) containing normal-state electrons.

Physically, the composites consist of amorphous germanium and polycrystalline niobium layers which form a stable, well-defined superlattice. Although knowledge of the germanium layers remains limited, they appear to effectively serve as electron tunnel barriers between Nb layers and have a characteristic tunneling length of 8 Å. Because the germanium is amorphous and effectively electrically insulating, the properties of the niobium layers are immediately separable.

The Read camera has clearly shown that the structure of the Nb layers changes markedly in the vicinity of 30 Å. Thicker layers show a strong (110) preferred orientation, while films thinner than 30 Å are distinctly disordered. The rate of change of the niobium film conductivity for thicker films is representative of usual bulk behavior, while the data for films thinner than 30 Å indicate much higher resistivities. Consistent with these results is a two-component view of the Nb layers in which each is composed of a fraction of bulklike material on one or both interfacial surfaces of which is a fixed thickness of disordered, low T_c material totaling roughly 30 Å.

Both niobium and germanium layer thicknesses are found to have a strong and systematic effect on the critical temperatures of the composites. In the limit of large germanium thickness, the decrease in T_c with D_{Nb} is in good accord with previous results for single Nb films. Surprisingly, however, at fixed D_{Nb} a steady and substantial rise in T_c is observed as D_{Ge} is decreased. The behavior of T_c in the large D_{Ge} limit can be explained by a proximity effect between the proposed two components of each Nb film, as discussed above. We do not have a definitive explanation for the rise in T_c as $D_{Ge}\rightarrow 0$, although it may be related to improved crystal growth as the internal interfaces are removed. In summary then, although a fully detailed picture of the Nb/Ge composites remains to be completed, this initial study shows them to be stable superlattices of overall quite satisfactory integrity, the important parameters of which, such as layer thickness, periodicity, T_c, etc., are reproducible, well defined, and can be accurately determined.

The purpose of this paper has been to explicitly demonstrate a system of variable superconducting dimensionality. This has been done by a study of their parallel upper critical fields and fluctuation conductivity. The hope is that this family of synthetic superlattices can be employed to explore a wide range of dimension-dependent superconducting phenomena and may also provide easy and flexible access to other superconducting states unique to this geometry.

ACKNOWLEDGMENTS

We would like to thank D. Keith for his patient, able assistance in the preparation of our layered samples and W. Knorr for his crafting of the beautiful cryostat with which our critical-field measurements were conducted. Scientific thanks must go to T. H. Geballe and T. P. Orlando for their continuing aid in helping us understand layered superconductors. This work was supported by the National Science Foundation, both directly for the physical property studies and through the Center of Materials Research here at Stanford, at which our samples were prepared. One of us (S.T.R.) would like to acknowledge the support of the Office of Naval Research at Yale University during the final stages of preparation of this paper.

APPENDIX: PROXIMITY-EFFECT THEORIES

1. de Gennes—Werthammer theory

In a modified version of the de Gennes theory,[26] Werthammer has shown[27] that in the dirty limit the T_c of a bilayer of two films with different T_c's can be written implicitly as

$$\ln t_S = \psi\left[\frac{1}{2}\right] - \psi\left[\frac{1}{2}+\frac{y_S}{2t_S}\right],$$
$$\ln t_N = \psi\left[\frac{1}{2}\right] - \psi\left[\frac{1}{2}-\frac{y_N}{2t_N}\right], \quad \text{(A1)}$$

where

$$t_S \equiv T_c/T_{cS} \le 1, \quad t_N \equiv T_c/T_{cN} \ge 1,$$

and

$$y_S \equiv \frac{4}{\pi^2} q_S^2 \xi_S^2(0), \quad y_N \equiv \frac{4}{\pi^2} q_N^2 \xi_N^2(0), \quad \text{(A2)}$$

with the boundary-imposed condition that

$$q_S \tan q_S D_S = \eta q_N \tanh q_N D_N . \quad \text{(A3)}$$

Here $\psi(x)$ represents the digamma function.[28] Therefore, the new T_c of the bilayer system is given by (A1) under the constraint of (A3), where T_{cS} and T_{cN} represent the critical temperatures of the superconducting and normal (lower T_c) films. D_S and D_N represent the thickness of the films and $\xi(0)$ is the Ginzburg-Landau coherence length. η characterizes the boundary conditions on the problem. It is given by de Gennes[29] as

$$\eta = \frac{N_N(0)D_N}{N_S(0)D_S} = \frac{\sigma_N}{\sigma_S}, \quad \text{(A4)}$$

where in Eq. (A4) $D = v_F l/3$ (not the film thickness) and σ is the conductivity.

Assuming a perpendicular magnetic field does not change (A3), the effect of such a field can be included by letting

$$q_S^2 \to q_S^2 + q_H^2$$

and (A5)

$$q_N^2 \to q_N^2 - q_H^2$$

in Eq. (A2), where

$$q_H^2 = 2\pi H/\Phi_0 \quad \text{(A6)}$$

accounts for the pairbreaking effect of the field. The slope of the upper critical field is thus given by

$$\left.\frac{dH_{c2\perp}}{dT}\right|_{T_{cNS}} T_{cNS} = \frac{4\Phi_0}{\pi} \frac{t_N - t_S}{\xi_N^2(0)(1-t_S)\psi'(\frac{1}{2}-y_N/2t_N) + \xi_S^2(0)(t_N-1)\psi'(\frac{1}{2}+y_S/2t_S)}, \quad \text{(A7)}$$

where

$$\psi'(z) \equiv \frac{d}{dz}\psi(z) .$$

Note that $\psi'(\frac{1}{2}) = \pi/2$.

Finally, if $D_S/\xi_S(0) \ll 1$ and $D_N/\xi_N(0) \ll 1$, we obtain

$$\frac{1}{T_{cNS}} = \frac{\frac{D_s}{\xi_S^2(0)}\frac{1}{T_{cS}} + \eta\frac{D_N}{\xi_N^2(0)}\frac{1}{T_{cN}}}{\frac{D_S}{\xi_S^2(0)} + \eta\frac{D_N}{\xi_N^2(0)}} \quad \text{(A8)}$$

and

$$\left.\frac{dH_{c2}}{dT}\right|_{T_{cNS}} T_{cNS} = \frac{\Phi_0/2\pi}{D_S + \eta D_N}\left[\frac{D_S}{\xi_S^2(0)} + \eta\frac{D_N}{\xi_N^2(0)}\right]. \quad \text{(A9)}$$

2. Cooper limit

An alternative result for T_c in the limit of $D_S/\xi_S(0) \to 0$ and $D_N/\xi_N(0) \to 0$ (assuming $\langle\omega\rangle_S = \langle\omega\rangle_N$) is given by the Cooper theory. In de Gennes's revised version of the Cooper theory,[29] λ, the electron-phonon coupling constant, is represented as an averaged value as

$$\bar{\lambda} = \overline{NV} = \frac{\lambda_N[N_N(0)D_N] + \lambda_S[N_S(0)D_S]}{N_N(0)D_N + N_S(0)D_S} . \quad \text{(A10)}$$

T_c can then be calculated from the formula of McMillan[30] and Allen and Dynes,[31]

$$T_c = \frac{\omega_{\log}}{1.2}\exp\left[\frac{-1.04(1+\lambda_{ep})}{\lambda_{ep} - \mu^*(1+0.62\lambda_{ep})}\right], \quad \text{(A11)}$$

where in the work reported here we have taken $\omega_{\log} = 142$ K and $\mu^* = 0.097$.[32]

*Present address: Section of Applied Physics, Yale Unversity, New Haven, CT 06520.

[1]T. W. Haywood and D. G. Ast, Phys. Rev. B 18, 2225 (1978).

[2]S. T. Ruggiero, T. W. Barbee, and M. R. Beasley, Phys. Rev. Lett. 45, 1299 (1980).

[3]H. Raffy, E. Guyon, and J. C. Renard, Solid State Commun. 14, 427 (1974); 14, 431 (1974); see also R. E. Howard, M. R. Beasley, T. H. Geballe, C. N. King, R. H. Hammond, R. H. Norton, J. R. Salem, and R. B. Zubeck, IEEE Trans. Magn. 13, 138 (1977).

[4]C. G. Granquist and T. Claeson, Solid State Commun. 32, 531 (1979).

[5]I. Banerjee, Q. S. Yang, C. M. Falco, and I. K. Schuller, Solid State Commun. 41, 805 (1982); I. K. Schuller, Phys. Rev. Lett. 44, 1597 (1980); see also J. Geerk, M. Gurvitch, D. B. McWhan, and J. M. Rowell, Bull. Am. Phys. Soc. 26, 441 (1981).

[6]W. Lawrence and S. Doniach, in *Proceedings of the 12th International Conference on Low-Temperature Physics, Kyoto,* edited by Eizo Kanda (Academic, Tokyo, 1971), p. 361.

[7]R. A. Klemm, A. Luther, and M. R. Beasley, Phys. Rev. B 12, 877 (1975).

[8]S. Foner and E. J. McNiff, Phys. Lett. 45A, 429 (1973).

[9]D. E. Prober, R. E. Schwall, and M. R. Beasely, Phys. Rev. B 21, 2717 (1980).

[10]J. A. Woollam, R. B. Somoano, and P. O'Connor, Phys. Rev. Lett. 32, 712 (1974).

[11]T. W. Barbee, Jr. and D. Keith, Stanford University Synchrotron Radiation Research Laboratory Report No. 78-04 (unpublished).

[12]M. H. Read, Thin Solid Films 10, 123 (1972).

[13]E. F. Kaelble, *Handbook of X rays* (McGraw-Hill, New York, 1965).

[14]L. J. van der Pauw, Philips Res. Rep. 13, 1 (1958).

[15]A. F. Mayadas, R. B. Laibowitz, and J. J. Cuomo, J. Appl. Phys. 43, 1287 (1972); S. A. Wolf, J. J. Kennedy, and M. Nisenoff, J. Vac. Sci. Technol. 13, 145 (1976).

[16]A broad discussion of this issue is presented by W. Silvert, J. Low Temp. Phys. 20, 439 (1975).

[17]R. C. Dynes and C. M. Varma, J. Phys. F 6, L215 (1976).

[18]N. R. Werthammer, E. Helfand, and P. C. Hohenberg, Phys. Rev. 147, 295 (1966).

[19]R. Klein and G. Fischer, Phys. Rev. 150, 222 (1966).

[20]D. A. Rudman and M. R. Beasely, Appl. Phys. Lett. 36, 1010 (1980).

[21]M. Tinkham, *Introduction to Superconductivity* (McGraw-Hill, New York, 1975).

[22]K. Yamafuji, T. Kawashima, and F. Irie, Phys. Lett. 20, 122 (1966).

[23]These data were discussed in a presented paper by Q. S. Yang, I. Banerjee, Charles M. Falco, and Ivan K. Schuller, Bull. Am. Phys. Soc. 27, 215 (1982).

[24]D. Saint-James, G. Sarma, and E. J. Thomas, *Type II Superconductivity* (Pergamon, New York, 1969).

[25]K. Yamafuji, E. Kusayanagi, and F. Irie, Phys. Lett. 21, 11 (1966).

[26]G. Deutscher and P. G. de Gennes, in *Superconductivity,* edited by R. D. Parks (Dekker, New York, 1969), Vol. II, p. 1005.

[27]N. R. Werthammer, Phys. Rev. 132, 2440 (1963).

[28]M. Abramowitz and I. A. Stegun, *Handbook of Mathematical Functions* (U.S. GPO, Washington, D.C., 1974); I. S. Gradshteyn and I. M. Ryzhik, *Table of Integrals, Series and Products* (Academic, New York, 1965).

[29]P. D. de Gennes, Rev. Mod. Phys. 36, 225 (1964).

[30]W. L. McMillan, Phys. Rev. 167, 331 (1968).

[31]P. B. Allen and R. C. Dynes, Phys. Rev. B 12, 905 (1975).

[32]E. L. Wolf and R. J. Noer, Solid State Commun. 30, 391 (1979).

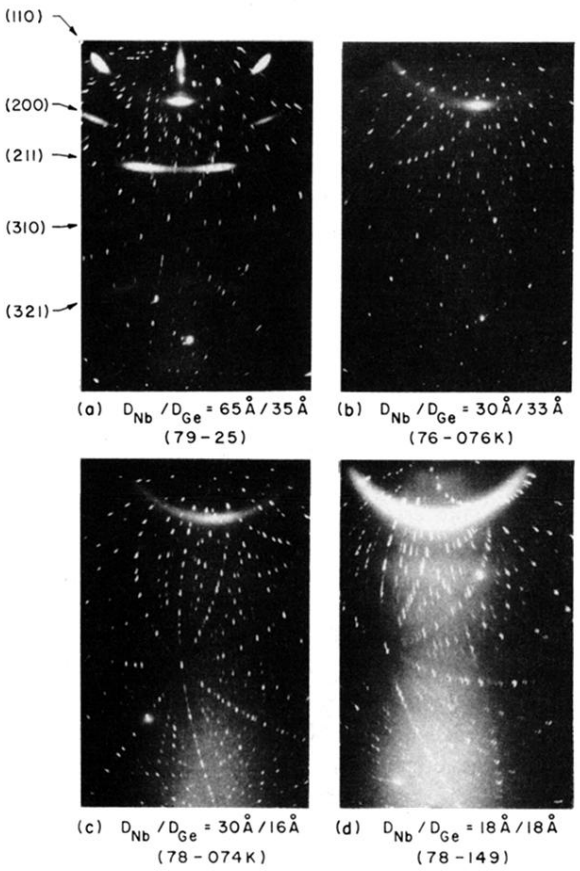

FIG. 2. Representative Read camera x-ray photographs of Nb/Ge composites. The small dots are reflections from the sapphire substrates; the symmetric arcs are identified with bcc Nb lattice reflections. Features of the amorphous Ge layers are not apparent here. The Nb layer are polycrystalline and in samples *A* and *B* exhibit a high degree of preferred orientation of the (110) plane parallel to the film surface. Samples *C* and *D* contain more disordered Nb films.